

Directional locking effects and dynamics for particles driven through a colloidal lattice

C. Reichhardt and C. J. Olson Reichhardt

Center for Nonlinear Studies and Theoretical Division, Los Alamos National Laboratory, Los Alamos, New Mexico 87545, USA

(Received 2 December 2003; published 30 April 2004)

We examine the dynamics of a single colloidal particle driven through a colloidal lattice which can distort in response to the driven particle. We find a remarkably rich variety of dynamical locking phenomena as we vary the angle of the applied drive with respect to the orientation of the colloidal lattice. When the driven colloid locks to certain lattice symmetry directions, its motion is not necessarily aligned with the drive. Applying a transverse force to the driven particle can result in either increased or decreased drag in the driving direction, depending on the angle of the drive. The dynamical locking produces anomalies in both the longitudinal and the transverse velocity vs driving force curves, including steps and regimes of negative differential resistance. As the interaction of the driven particle with the surrounding lattice increases, significant distortion or dislocations in the surrounding media occur, and as a result the directional locking is enhanced. We compare these results to those obtained for driving particles over *fixed* substrates, and show that a far richer variety of behaviors occurs when the underlying lattice is allowed to distort. We discuss how this system can be used for particle species segregation when the onset of different locking angles occurs at different drives for varied particle charges. We also show that the most pronounced locking phases should be observable at temperatures up to the melting transition of the colloidal lattice.

DOI: 10.1103/PhysRevE.69.041405

PACS number(s): 82.70.Dd, 05.45.-a

I. INTRODUCTION

Assemblies of interacting colloidal particles exhibit a wide range of ordered, glassy, and liquid states [1,2], and have proven an ideal system for studying these equilibrium states with various imaging techniques. Colloids can also be studied in nonequilibrium conditions such as under shear or when driven with different types of fields [2]. Recently Korda *et al.* [3] investigated the dynamics of moving colloids driven over a square two-dimensional (2D) optical tweezer array. Here, the optical tweezers act as attractive sites [4]. In this system, a series of locked transport states occur as the angle at which the colloids are driven with respect to the optical lattice is varied. In the locked states, the colloids move along a high-symmetry direction of the lattice even when this is not the same as the direction of drive. The locking produces steps in the colloidal velocity vs driving angle, and may have applications as a novel method for continuous separation of particles of different species, such as macromolecules and biological cells [5–7]. Separation can be achieved when a particular species locks to a symmetry direction while the remaining species continue to move in the direction of the applied drive. Other techniques to separate particle species along this line include the transport of particles through periodic obstacle arrays [8,9].

Particle transport through fixed periodic arrays under varying drive direction has also been investigated in simulations of vortices moving in nanostructured superconductors [10,15] and Josephson junctions [11–13]. Recent experiments on vortices driven at different angles through periodic pinning arrays find guiding effects similar to the features seen in simulations [14]. Similar effects have also been studied in electron transport through periodic antidot arrays [16] as well as atomic friction over ordered surfaces [17]. In general, for all of these systems, the particle motion locks to certain symmetry angles of the lattice. References [10,16]

showed that the velocity vs angle curve has a devil's staircase structure, with a step in the particle velocity at each locking angle. Certain highly symmetrical angles of drive produce stronger locking than others.

In the experiments of Ref. [3] and the theoretical studies of Refs. [10–13,16,17], the periodic lattice through which the particles move is completely *rigid*. Another approach which has not been previously considered is for the driven particle to move through a stationary, but *distortable*, lattice of particles. In this case, the driven particle still interacts with a periodic array of obstacles; however, the driven particle can in turn affect the surrounding media and distort or create dislocations in the surrounding lattice. A physical example of such a system would be driving a single or small number of colloidal particles through a triangular colloidal lattice. This can be achieved by placing a colloidal particle that responds to an external drive into a colloidal lattice for densities and temperatures where the nondriven colloids form a triangular lattice. It should be straightforward to drive individual colloids with an optical tweezer [7]. It is also possible to use magnetic impurity particles driven with a magnetic field, as in recent experiments by Weeks and co-workers [18]. A variation on this type of system would be to have one colloid or impurity particle fixed at a spot and to drive the colloidal lattice past it. Experiments along this line have been performed previously for large obstacles [19].

A system that has many similarities to colloids is vortices in superconductors, where the mutual repulsion between vortices leads to the formation of a triangular lattice. For a clean superconductor where the intrinsic pinning is not strong enough to distort the vortex lattice, it may be possible to drive a single vortex with a magnetic force microscope or scanning tunneling microscope tip. It has also been demonstrated experimentally using a lithographically created artificial pin [20] that a single pinning site can capture one or more vortices while the other vortices are driven past. Other

similar systems include driving an obstacle through a triangular bubble raft lattice, or manipulating a single droplet of a two-ferrofluid system in a triangular droplet state. Another system closely related to colloids is 2D dusty plasmas where charged dust particles form a triangular lattice [21] and individual particles can be driven with lasers.

In a system where the periodic lattice through which a particle is driven can itself be affected by the driven particle, a number of intriguing scenarios are possible which cannot arise when the substrate is completely rigid. Examples include a transition from an ordered flow, where the driven particle only distorts the lattice elastically and does not create dislocations, to a disordered flow, where the particle tears the lattice and dislocations are generated. This could occur when the particle moves at an angle that is not commensurate with the lattice, or for a large enough driven particle. Other effects that could occur include the possibility that, for certain driving directions, the driven particle may drag portions of the nondriven lattice with it. Conversely, for other driving directions, the particle may be able to slip freely between the particles comprising the lattice. Since the lattice can locally distort to more easily accommodate the motion of the driven particle in the locked regimes, the locking effects may be different in nature and more pronounced than those observed in previous work on rigid substrates. One practical application of this system, as suggested in Refs. [3,5], is the continuous separation of different species of particles as they move through periodic arrays of obstacles. We demonstrate that the separation of particles of different charges is enhanced by the ability of the surrounding lattice to distort. If, under certain conditions, the distortable lattice can act as a filter for different charged particles, then the additional step of using optical tweezer arrays, as in Ref. [3], would not be needed.

II. SIMULATION

We simulate a 2D monodisperse colloidal assembly using Langevin dynamics, with techniques that have been described previously [22,23]. The overdamped equation of motion for a single colloid i in a system with periodic boundaries in the x and y directions is

$$\eta \frac{d\mathbf{r}_i}{dt} = \mathbf{f}_{ij} + \mathbf{f}_d^i + \mathbf{f}_T. \quad (1)$$

Here $\eta=1$ is the damping term arising from the fact that the particle is moving through a viscous media. The interaction force from the other colloids is $\mathbf{f}_{ij} = -\sum_{j \neq i}^N \nabla_i V(r_{ij})$, where the repulsive colloid-colloid interaction is Yukawa or screened Coulomb,

$$V(r_{ij}) = \frac{q_i q_j}{|\mathbf{r}_i - \mathbf{r}_j|} \exp(-\kappa |\mathbf{r}_i - \mathbf{r}_j|). \quad (2)$$

Here $q_{i(j)}$ is the charge of the particle, $1/\kappa$ is the screening length, \mathbf{r}_i is the position of particle i , and \mathbf{r}_j is the position of particle j . We initialize the system in a triangular lattice with N colloids and a lattice constant a , and then insert one

additional driven colloid. The screening length is fixed at $1/\kappa=3a$.

The thermal force \mathbf{f}_T is a randomly fluctuating force modeled as random kicks, with the properties $\langle \mathbf{f}_T(t) \rangle = \mathbf{0}$ and $\langle \mathbf{f}_T(t) \mathbf{f}_T(t') \rangle = 2\eta k_B T \delta(t-t')$. For most of the results presented here, the colloid density is held fixed and the system size is set to $L=34a$. With these parameters there is a well-defined melting temperature T_m for the unperturbed lattice, which we determine by measuring the fraction of colloids which are sixfold coordinated, P_6 . In the solid, $P_6=1$, but at the melting transition T_m , defects proliferate and P_6 falls below 1 and becomes noisy [24]. We measure temperature in units of T_m . For the first part of the paper we consider the case of $T=0$ so that the effects of the dynamics can be clearly distinguished. We later show that for a large range of T/T_m essentially the same results appear, and that the locking effects are lost for $T/T_m > 1$. Thus the results from our work should be applicable to experimental samples at finite temperatures.

We vary the charge on the driven particle q_d and the direction of drive. All particles except the driven one have charge $q=1$ and applied dc drive $\mathbf{f}_d^i=0$. The force on the driven particle has two components:

$$\mathbf{f}_d = f_x^d \hat{\mathbf{x}} + f_y^d \hat{\mathbf{y}}. \quad (3)$$

We hold f_x^d fixed at a constant value and increase f_y^d . We then monitor the velocities V_x and V_y of the driven particle.

We do not take into account possible hydrodynamic effects or possible long-range attractions between colloids. We have conducted simulations for different system sizes, lattice constants a , and screening lengths, and find that the qualitative results presented here are robust.

III. SMALL DRIVEN PARTICLE

We first consider the case where the driven particle interacts only weakly with the surrounding particles so that, although small distortions of the lattice can occur, no dislocations are formed in the surrounding media. We define this weak interaction regime as $q_d/q < 0.5$. In the case of a triangular lattice aligned in the x direction, as in Fig. 1(a), locking should occur for angles of drive where the driven colloid can move freely between the colloids in the lattice. This occurs for ratios of the applied drive of

$$\frac{f_y^d}{f_x^d} = \frac{\sqrt{3}m}{2n+1}, \quad (4)$$

where m and n are integers. The corresponding locking angle is $\theta = \arctan(f_y^d/f_x^d)$. Equation (4) predicts locking at 60° corresponding to $m=1, n=0$; 30° corresponding to $m=1, n=1$; 19.1° corresponding to $m=1, n=2$; and 0° for $m=0$. Other locking angles occur for higher-order values of m and n . In Fig. 1 we illustrate the driven particle, the surrounding lattice, and the particle trajectories for a system with fixed parameters of $q_d/q=0.35$ and $f_x^d=1.0$ for increasing $f_y^d/f_x^d=0, 0.57$, and 0.78 . The trajectories in all these cases show that the driven particle moves through the lattice without significantly distorting it, due to the weak charge of the driven particle. In Fig. 1(a) we show

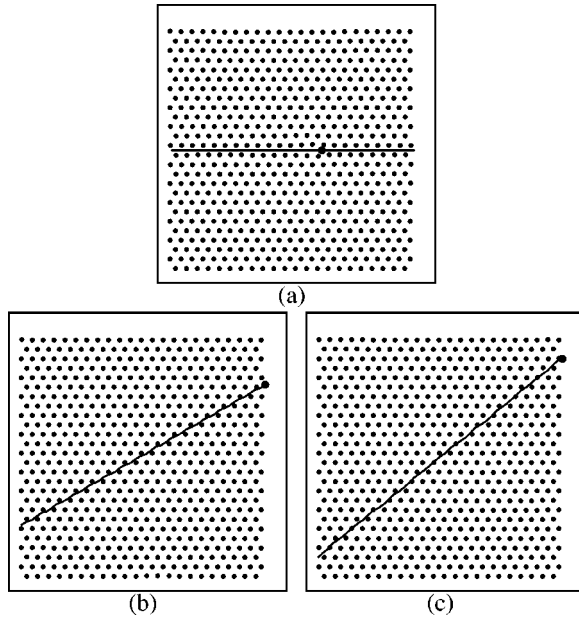


FIG. 1. Particles (black dots) and trajectories (black lines) for a system with $q_d/q=0.35$ at $f_x^d=1.0$ and (a) $f_y^d/f_x^d=0.0$, (b) 0.57, and (c) 0.78.

the commensurate case of $f_y^d/f_x^d=0$ where the particle channels between the surrounding colloids. Figure 1(b) presents another commensurate case for $f_y^d/f_x^d=0.57$ where the particle moves in a periodic orbit along a symmetry line of the lattice. This orbit corresponds to $m=1, n=1$ from Eq. (4), so the flow is along 30° . In Fig. 1(c) we show an incommensurate case of $f_y^d/f_x^d=0.78$, which is not a simple ratio in Eq. (4). Here the particle does not move in a completely periodic orbit but shows some nonperiodic deviations; however, the particles in the surrounding lattice still show little deviation from their positions. We observe similar types of motion at the other incommensurate angles as well.

In order to better demonstrate the difference between the commensurate and incommensurate particle orbits in Fig. 1, we analyze the power spectra of the velocity V_y of the driven particle for the two cases. In Fig. 2 we show the power spectra $S(\nu)$ obtained from a time series of V_y of the driven particle at fixed f_y^d/f_x^d . Figure 2(a) illustrates $S(\nu)$ for the commensurate case $f_y^d/f_x^d=0.57$ shown in Fig. 1(b). Here the spectrum has a prominent peak at $\nu=0.0127$ inverse molecular dynamics steps with higher harmonics, indicating that the particle motion is strictly periodic with a single frequency. In a commensurate orbit, a single frequency is expected to appear since the particle is moving along a symmetry direction of the lattice and is slowed by the interactions from the surrounding lattice at a constant spacing and a constant rate. In Fig. 2(b), the spectrum for the incommensurate case $f_y^d/f_x^d=0.78$ shown in Fig. 1(c) has many peaks, indicating that the particle is undergoing motion with many different periods giving a broad spectrum. In general, for these incommensurate phases, the particle likely jumps between several different closely spaced locked phases with high m and n values which, together, produce an angle of motion which is close

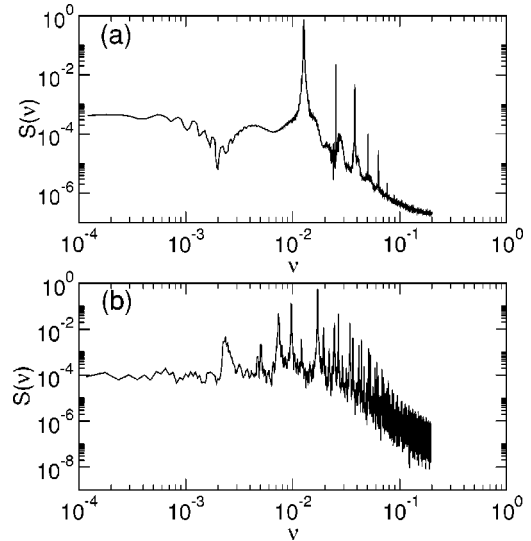


FIG. 2. The power spectra obtained from a time series of V_y for (a) the commensurate case $f_y^d/f_x^d=0.57$ shown in Fig. 1(b) and (b) the incommensurate case $f_y^d/f_x^d=0.78$ shown in Fig. 1(c).

to the angle of the drive. We find similar behaviors in the power spectra at other commensurate and incommensurate angles.

In Fig. 3(a) we simultaneously plot V_x and V_y vs f_y^d/f_x^d , with fixed $f_x^d=1.0$, showing that the locked phases strongly affect the transport properties. We highlight a few ratios of (m, n) from Eq. (4) to indicate the most prominent locking phases: $(0, 0)$, which starts at $f_y^d/f_x^d=0$ in the bottom left corner of Fig. 3(a); $(1, 1)$ for flow at 30° ; and the very prominent $(1, 0)$ locking centered at $f_y^d/f_x^d=1.7$. There are additional smaller steps that are difficult to see for this value of q_d . Another interesting feature is that V_x has an average value of 0.9 for $f_y^d/f_x^d < 2.0$. We note that, for a single driven colloid moving in the absence of any other particles, we would have $V_x=1.0$, which is higher than the value obtained in the presence of the other particles. This indicates that the driven particle experiences an additional damping due to the interactions with the other particles. This damping originates when the surrounding colloids shift slightly as the driven particle moves past. Since the motion of these surrounding colloids is also overdamped, the only source of energy is the driven particle. In the case of a rigid substrate [10], this additional damping effect is absent since the periodic substrate cannot distort and absorb energy. Another immediately obvious difference between this system and particle motion over a rigid substrate is that in Fig. 3(a), none of the steps in V_y have $dV_y/df_y^d=0$ [1,10,16]. Although the slope of V_y is reduced on the steps, it does not drop to zero, indicating that along the locking directions the particle velocity V_y continues to increase with f_y^d . Figure 3(a) also indicates that, in the locking regions, V_x is not constant but shows features where the velocity both *increases* and *decreases* which coincide with slope changes in V_y . On the steps, when V_y locks to the lower slope value, V_x locks to a constant positive slope which can be seen most clearly near $f_y^d/f_x^d=1.7$ at the 60° locking of $(1, 0)$. At the lower edge of the $(1, 1)$ and $(1, 0)$ steps, V_x *decreases* in an abrupt dip before rising linearly on

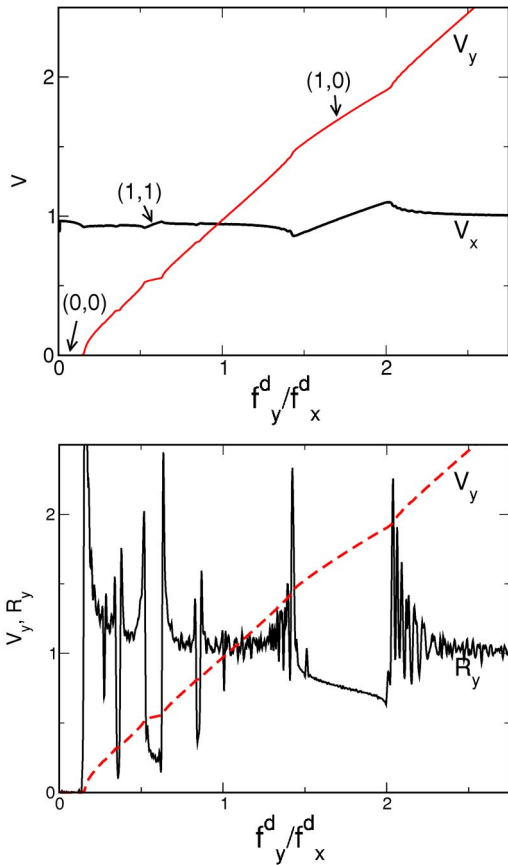


FIG. 3. (a) V_x (dark line) and V_y (light line) for fixed $f_x^d=1.0$ and increasing f_y^d for $q_d/q=0.35$. (b) V_y (dashed line) and its derivative R_y (solid line), showing the locking phases more clearly.

the step. On the upper end of these steps, when the slope in V_y increases again, V_x shows another decrease.

In Fig. 3(b) we plot V_y along with its derivative R_y to show the locking phases more clearly. At the (1,0) locking, R_y drops to a lower value due to the smaller slope of V_y in the locking regions. Peaks appear in R_y at the beginning and end of each locked phase, reflecting the increased slope of V_y outside of the locked regions. R_y also shows some oscillations above the (1,0) locking, which we discuss in more detail in Sec. IV C. Additionally, locking phases appear as dips in R_y for the (1,1) locking centered at $f_y^d/f_x^d=0.57$ as well as at (1,2) and (1,3).

Figure 3(a) also demonstrates that there is a clear *transverse depinning* threshold for the (0,0) locking: $V_y=0.0$ for $f_y^d/f_x^d < 0.15$. Here, despite the fact that the particle is moving in the x direction, there is an effective pinning threshold for motion in the y direction. Below this depinning threshold, the particle trajectories are the same as those shown in Fig. 1(a), where the particle moves in an effective 1D trough. Transverse depinning thresholds have been observed in various systems of particles driven longitudinally over a 2D periodic substrate as an increasing transverse force is applied. These systems include longitudinally moving vortices in periodic pinning arrays [10,11,13] and atoms moving over periodic surfaces [17]. In colloidal experiments on periodic substrates, a locking is observed for small angles [3]. In all

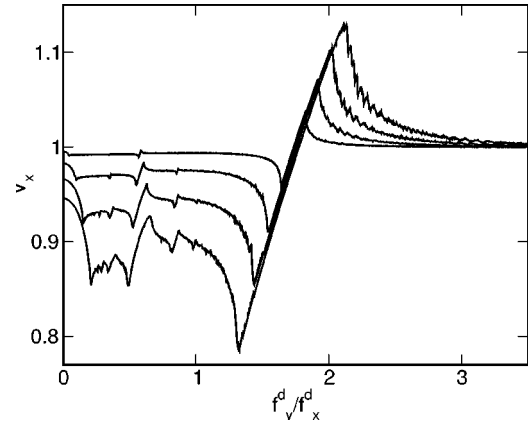


FIG. 4. V_x vs f_y^d/f_x^d for $q_d/q=0.125, 0.25, 0.35$, and 0.5 (from top left to bottom left).

these cases the particle motion remains locked in the longitudinal direction until a large enough transverse force is applied. In Fig. 3(a) as f_y^d/f_x^d approaches the transverse depinning threshold, V_x , the particle velocity in the x -direction, decreases. This decrease occurs because the increasing transverse force shifts the driven particle closer to the lattice particles, increasing the interaction between the driven particle and the other particles. Since the surrounding lattice is flexible, some of the motion of the driven particle is transferred into small distortions of the surrounding lattice. These distortions increase as the driven particle is forced closer to the particles in the lattice. Once the driven particle begins to move in the y direction, its velocity in the x direction increases since the driven particle no longer approaches the particles in the surrounding lattice as closely and thus experiences less damping of its motion. Remarkably, for $1.8 < f_y^d/f_x^d < 2.0$, V_x is *greater* than 1.0, indicating that the particle is moving *faster* than it should given the applied driving force in the x direction. This indicates that some of the energy from the y component of the drive is being transferred to the x direction. Above the (1,0) step for $f_y^d/f_x^d > 2.0$, V_x decreases slowly back to 1.0.

We next consider how the locking regions evolve with increasing q_d . In Fig. 4 we plot V_x vs f_y^d/f_x^d for $q_d/q = 0.125, 0.25, 0.35$, and 0.5 with $f_x^d=1.0$. The plots are overlaid with no offset. For $f_y^d/f_x^d=0$, V_x decreases for increasing q_d , indicating that the damping increases as q_d rises. This decrease in V_x occurs because the driven particle interacts more strongly with the surrounding particles, causing larger distortions and transferring more of its energy into the lattice. Additionally, all of the locking phases become wider with increasing q_d , indicating that as the distortions in the surrounding lattice from the driven particle increase, the channeling effect becomes stronger. The locking phases for the higher-order values of (m,n) can now be clearly resolved, especially for the $q_d/q=0.5$ curve where a particularly large number of dips occur for $f_y^d/f_x^d < 1.0$. For the locking at (1,0), the value of V_x exceeds 1.0 for $f_y^d/f_x^d > 1.7$ at all values of q_d . Just above the (1,0) locking, V_x decays back to 1.0. During this decay, there are clear small scale periodic peaks which are a real effect that we study later in this paper.

We note that for small q_d , the behavior of this system is similar to that of a particle moving through a rigid lattice in

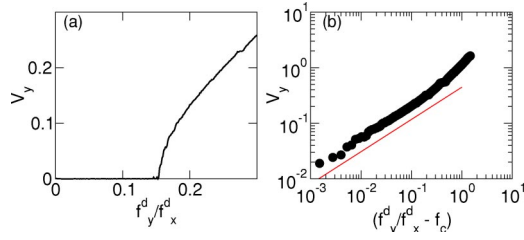


FIG. 5. (a) V_y vs f_y^d/f_x^d at the transverse depinning transition for the system shown in Fig. 3 with $q_d/q=0.35$. (b) Log-log plot of V_y vs $(f_y^d/f_x^d - f_c)$ where $f_c=0.15$ is the transverse depinning threshold. The solid line is a power-law fit with an exponent of $\beta=0.58$.

Ref. [10], where the same type of anomalous steps were observed in both V_x and V_y . The locations of the steps in Ref. [10] occurred for different values of f_y^d/f_x^d since the underlying lattice was square rather than triangular. Additionally, the slope of V_y along the steps was nearly zero in the rigid lattice, making V_y appear much more steplike. The similar behavior found here at small q_d occurs when the driven particle can no longer cause significant distortions in the surrounding lattice, rendering it effectively rigid.

Dynamics of transverse depinning

We now examine the initial transverse depinning transition in more detail. We first consider the shape of V_y vs f_y^d/f_x^d near the transverse depinning. For elastic media depinning in the presence of quenched disorder, theory predicts $V \propto (f^d - f_c)^\beta$, where f_c is the depinning threshold [25]. For a single-particle depinning from a sinusoidal substrate in 1D, $\beta = 1/2$. In 2D systems of collectively interacting particles where plastic deformation occurs at depinning, studies find scaling in the velocity force curves with $\beta > 1.5$ [26]. It is not known if there would be any scaling for the transverse depinning of a longitudinally moving particle. In Fig. 5(a) we show V_y near the onset of motion in the y direction for the system in Fig. 3 with $q_d/q=0.35$. We plot V_y vs $f_y^d/f_x^d - f_c$ on a log-log scale in Fig. 5(b), where $f_c=0.15$ is the transverse depinning force. We find a reasonable power-law fit with $\beta=0.58$ [solid line in Fig. 5(b)], close to the single-particle value of $\beta=1/2$. This indicates that the transverse depinning is elastic in nature, and that when the particle depins it does not induce tearing in the surrounding lattice.

For the steps above $(0,0)$, whenever the particle leaves a locked region, V_y shows curvature similar to that of the initial transverse depinning. This suggests that on the higher-order steps, when the particle is channeling along an easy flow direction, the particle is effectively pinned in the direction transverse to \mathbf{f}_d , rather than in the direction transverse to f_x^d . As f_y^d increases, the transverse force eventually becomes high enough for the particle to depin and begin moving at a new angle.

In Fig. 6 we plot the particle trajectories at the transverse depinning transition for the system shown in Fig. 5. In Fig. 6(a), just above the initial transverse depinning at $f_y^d/f_c = 1.05$, the particle stays locked along the x direction for about $16a$ before moving in the positive y direction to the next row. The particle moves in a staircase fashion. In Fig.

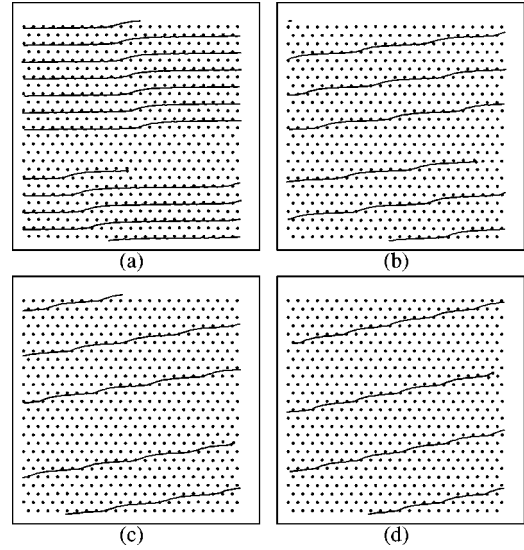


FIG. 6. Particles (black dots) and trajectories (black lines) near the transverse depinning transition for the system shown in Fig. 5 at $f_y^d/f_c=(a)$ 1.05, (b) 1.22, (c) 1.34, and (d) 1.5.

6(b) for $f_y^d/f_c=1.22$, we find a staircase motion similar to that of Fig. 6(a), but with the particle translating in the y direction every $7a$, producing a net V_y that is higher than that of Fig. 6(a). In Fig. 6(c) at $f_y^d/f_c=1.34$ and Fig. 6(d) at $f_y^d/f_c=1.5$, the staircase motion persists with the particle moving shorter distances in the x direction between jumps to the next row in the y direction.

IV. DRIVEN PARTICLES WITH INTERMEDIATE CHARGE

Next we consider the case for $0.5 < q_d/q < 3.0$, which we term the intermediate particle regime. Here we observe that the locking phases become more pronounced and appear more steplike in V_y with $dV_y/df_y^d=0$ in some places. We also find regimes where V_y decreases for increasing f_y^d , indicating a *negative* differential transverse resistance, or $dV_y/df_y^d < 0$. The scaling in the initial transverse depinning is also lost and is replaced by a sharp jump, indicating that for $q_d/q > 0.5$ the system is no longer in the elastic regime. In Fig. 7(a) we show V_x and V_y for a system with $q_d/q=1.0$. For these intermediate q_d values, the width of the $(1,0)$ locking becomes so large that it begins to overlap with the smaller locking phases, and some of the smaller locking steps are lost. The dips in V_x are more pronounced and there are several regions where both V_x and V_y show jumps into and out of different locked phases, rather than the smoother transitions seen for lower values of q_d . The slopes of V_x and V_y along the $(1,0)$ locking are both positive but show a nonlinear bowing effect. In Fig. 7(b) we plot V_x and V_y for $0 < f_y^d/f_x^d < 1$, showing the smaller locking phases more clearly. Along the step $(1,1)$, centered at $f_y^d/f_x^d=0.6$, the slope of V_y shows a bow feature, indicating that the slope becomes *negative* near $f_y^d/f_x^d=0.73$. On the next step we find a similar bow feature. This behavior is in contrast to the studies with rigid substrates, where the slope of V_y never drops below zero along the steps. Figure 7

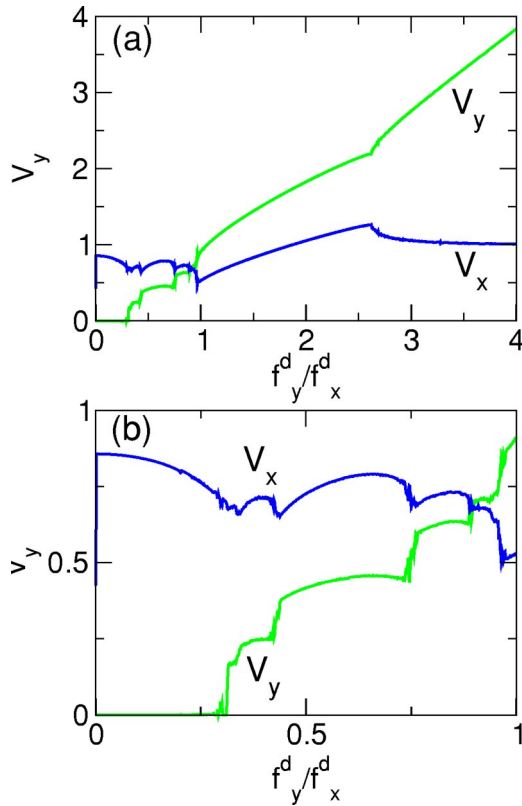


FIG. 7. (a) V_x (dark line) and V_y (lighter line) vs f_y^d/f_x^d for $q_d/q=1.0$. (b) Closeup of (a) for $0.0 < f_y^d/f_x^d < 1.0$.

also shows that both V_x and V_y can decrease simultaneously, indicating an overall increase in the damping. For these intermediate q_d values there is considerably more distortion in the surrounding lattice. Just before the driven particle exits a locked region, it has the strongest interaction with the surrounding media and experiences the largest damping. At the jumps in velocity accompanying each step, the driven particle can cause enough distortion to temporarily generate a localized dislocation in the lattice.

A. Trajectories in the locked phases

In Fig. 8 we illustrate some of the particle trajectories for different locking regimes from the system in Fig. 7. Figure 8(a) shows the step near $f_y^d/f_x^d=0.39$, which corresponds to the $m=1, n=2$ locking phase. The particle moves in a zigzag pattern. The elastic distortions in the surrounding colloid lattice are clearly visible in the form of very small loops on both sides of the path of the driven particle. Here, the colloids closest to the driven particle move a distance less than a as the driven particle approaches, and then return to their initial positions after the driven particle passes. There are some additional smaller distortions in the lattice at larger distances from the driven colloid; however, these motions are too small to be visible at the resolution in Fig. 8. In general, when the intermediate charged particles move through a channel during a locked phase, the motion is elastic and no dislocations are generated. Only during the transitions out of the locked phases do temporary distortions greater than a in the surrounding lattice occur.

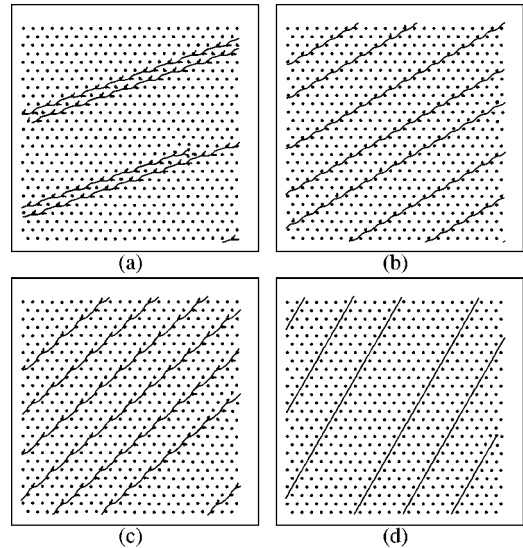


FIG. 8. Particles (black dots) and trajectories (black lines) for the system in Fig. 7 with $f_y^d/f_x^d=(a) 0.39$, (b) 0.6, (c) 0.8, and (d) 2.0.

Figure 8(b) shows the trajectories at $f_y^d/f_x^d=0.6$, when the particle moves at 30° in the $(1,1)$ locking regime. The width of this $(1,1)$ locked region is considerably larger than that of the $(1,2)$ phase in Fig. 8(a). Here, the particle follows a sinusoidal path and causes distortions in the surrounding lattice; however, these distortions are of a smaller magnitude than those in Fig. 8(a), indicating that the particle channels more easily on the $(1,1)$ step. In Fig. 8(c) we plot the trajectories for the step region at $f_y^d/f_x^d=0.8$, where more significant distortions in the surrounding lattice occur than for Fig. 8(b). The width of this step is smaller than the $(1,1)$ step in Fig. 8(b). In Fig. 8(d) we show the trajectories at $f_y^d/f_x^d=2.0$ for the most prominent step, $(1,0)$, where the vortices channel at 60° . There are almost no distortions in the surrounding lattice. For a value of f_y^d/f_x^d just below the end of the $(1,0)$ phase, $f_y^d/f_x^d \approx 2.6$, significant distortions of the colloids to the upper left of the driven particle occur in the surrounding lattice, since the driven particle is pushed in this direction by the increasing f_y^d . When these distortions become large enough, the $(1,0)$ phase ends.

B. Locked phase evolution as a function of q_d

In Fig. 9 we plot V_y vs f_y^d/f_x^d for increasing values of q_d . From bottom to top, $q_d/q=0.75, 1, 1.5, 1.75$, and 2.0. In this range of q_d , the initial transverse depinning threshold changes little; however, the width of the $(1,0)$ locking which begins at $f_y^d/f_x^d \approx 1.1$ grows until it saturates at $q_d/q=1.75$. The width of the locking regions for $f_y^d/f_x^d < 1.1$ does not increase much with q_d ; however, they became increasingly smeared, which is particularly noticeable for $q_d/q \geq 1.75$. The smearing occurs when the lattice distortions become large enough to create dislocations in the surrounding lattice. These dislocations appear when the particle jumps from one symmetry angle to another, and thus they smear out the transition. The saturation of the width of the main $(1,0)$ step also

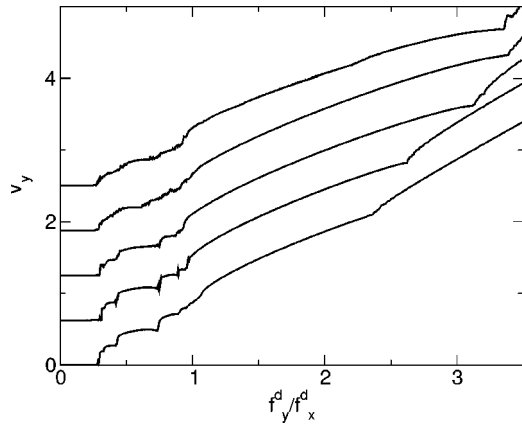


FIG. 9. V_y vs f_y^d/f_x^d for varied q_d/q . A systematic shift is added in the y direction for clarity. From top to bottom, $q_d/q = 2.0, 1.75, 1.5, 1.0,$ and 0.75 .

coincides with the onset of the creation of dislocations as the particle passes into and out of the locked phase. In Fig. 10 we plot the corresponding V_x vs f_y^d/f_x^d for the system in Fig. 9. Again we find a smearing of the features with increasing q_d for $f_y^d/f_x^d < 1.0$. Additionally, we find an increase in the magnitude of the fluctuations in V_x just above the end of the $(1,0)$ locking phase for $q_d/q = 2.0$, due to the formation of dislocations in the surrounding media.

In Fig. 11 we plot a phase diagram showing the evolution of the widths of the transverse pinned phase T_p and the $(1,0)$ locked phase L . The phases are identified from the features in V_y shown in Fig. 9. Here the transverse pinned phase T_p grows with q_d until its width saturates around $q_d/q = 0.75$, while the locked phase L also grows with q_d and saturates at $q_d/q = 1.75$. There is a small decrease in the width of the locked phase for higher values of q_d . Above $q_d/q = 2.5$, the phases become increasingly difficult to distinguish due to the large distortions in the lattice that cause large velocity fluctuations near the transitions into and out of the locked phases.

The $(1,0)$ phase grows with increasing particle interaction strength q_d because the driven particle can more easily dis-

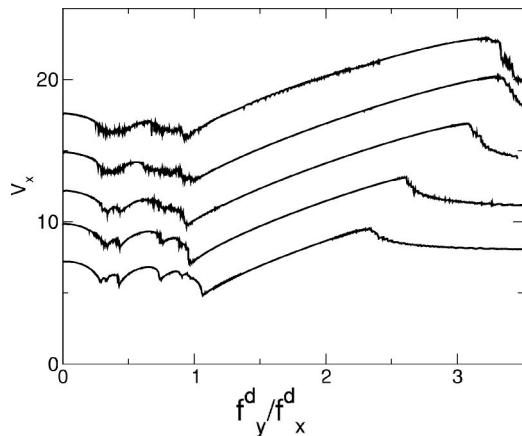


FIG. 10. V_x vs f_y^d/f_x^d for the system in Fig. 9 with a systematic shift added to the y direction for clarity. From top to bottom, $q_d/q = 2.0, 1.75, 1.5, 1.0,$ and 0.75 .

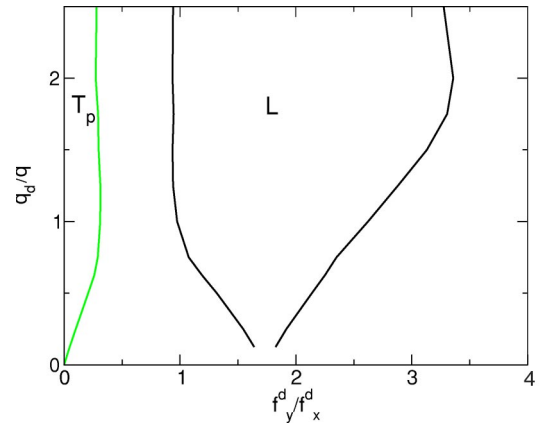


FIG. 11. Phase diagram for q_d/q vs f_y^d/f_x^d . The transverse pinned phase is marked T_p , and the locked phase for $m=1, n=0$ is marked L .

tort the surrounding lattice, allowing the lattice to accommodate the $(1,0)$ phase for larger angles between the driving force and 60° . The increasing size of the locked region can also be viewed as arising from the fact that, as q_d increases, the driven particle experiences a stronger potential interaction with the lattice. Eventually, for large enough q_d/q , the distortion in the surrounding lattice becomes strong enough to allow dislocations to be created, enabling the particle to jump out of the locked channel and limiting the growth of the locked phase L in Fig. 11. As the particle interaction increases above $q_d/q = 2$, this transition occurs at lower values of f_y^d/f_x^d and the width of the $(1,0)$ phase decreases as seen in Fig. 11. A similar growth of the size of the locked regions has been observed for systems with fixed lattices in Refs. [10,16].

The behavior of the locked phase in Fig. 11 also indicates how this system could be used for particle species separation. If two different species of particles are moving through the sample with the same applied f_y^d/f_x^d , then it is possible for one of the species to be in the locked L phase while the other species is not, and thus the two species will move in different directions. For example, for a drive of $f_y^d/f_x^d = 1.25$, particles with $q_d/q > 0.75$ are in the L phase while particles with $q_d/q < 0.75$ are not and will move at smaller angles. One advantage of this technique over the optical traps is that particles with the same optical properties but different charges or sizes could be separated.

C. Dynamics just outside of the $m=1, n=0$ phase

We now look more closely at some features in the V_x and V_y curves as well as the particle dynamics just at the end of the $m=1, n=0$ phase. In Fig. 10, after the end of the $(1,0)$ phase, the V_x curves decay back to $V_x = 1.0$. All the values $q_d/q < 2.5$ show a similar decay in this regime. To examine this decay, in Fig. 12(a) we plot $V_x - V_0$ vs $f_y^d/f_x^d - f_c$, where $q_d/q = 0.75$, $V_0 = 1.0$, and $f_c = 2.338$ is the driving force at which the $(1,0)$ locked regime ends and the V_x decay begins. In Fig. 12(b) we plot the same curve in log-linear form and show a good fit to an exponential form $A \exp(-bx)$, with b

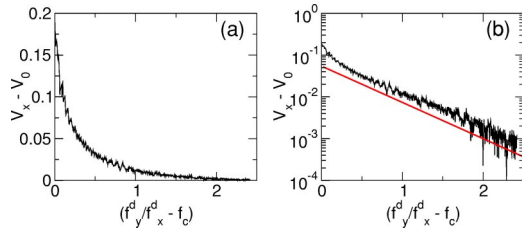


FIG. 12. (a) $V_x - V_0$ vs $f_y^d/f_x^d - f_c$, where $V_0 = 1.0$ and $f_c = 2.338$ is the value of the driving force when the $(1, 0)$ locking phase ends for a system with $q_d/q = 0.75$. (b) Log-linear plot of (a). The solid straight line is a fit with the form $A \exp(-bx)$ where $b = 2.0$ and $A = 0.1$.

$= 2.0$. For other values of q_d/q we observe the same behavior with similar values for b . The fitting constants and curve shape do not change when the drive is swept more slowly in the simulations, indicating that we are not observing a transient behavior.

In the decay region shown in Fig. 12, there appear to be some smaller oscillations in V_x . Similar oscillations are also seen in V_y . Focusing on this region, we find that the oscillations are actually steps. In Fig. 13(a) we plot V_y for the case of $q_d/q = 0.75$ right after the end of the $(1, 0)$ locked phase. Here V_y does not increase smoothly but passes through a series of small jumps. Between these jumps V_y increases linearly. In Fig. 13(b) we plot the corresponding V_x for the same range of driving forces. Here V_x also decreases in a series of jumps which coincide with the jumps in V_y . Between the jumps, V_x increases linearly. For higher values of f_y^d/f_x^d beyond what is shown in Fig. 13, the jumps continue and become more frequent until they overlap. In order to determine the cause of the steps, in Fig. 14 we plot the particle trajec-

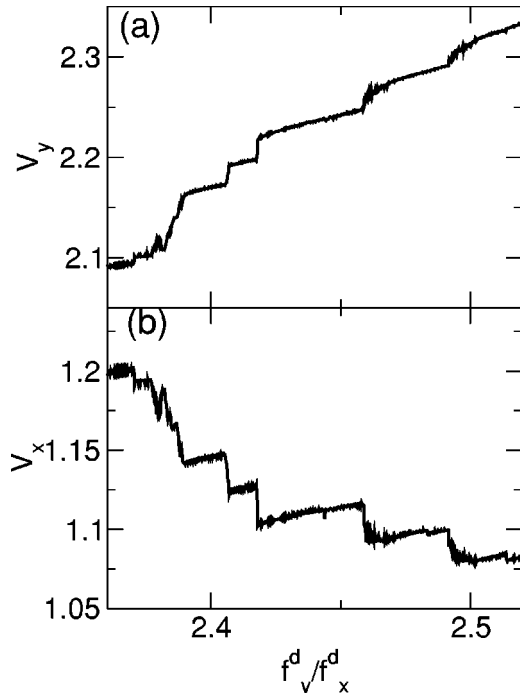


FIG. 13. (a) V_y vs f_y^d/f_x^d for the system in Fig. 12, just after the $(1, 0)$ locking ends. (b) Corresponding V_x .

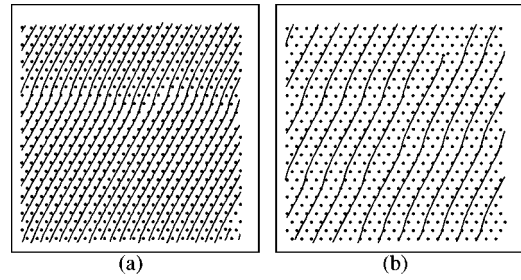


FIG. 14. Particles (black dots) and trajectories (black lines) for the system in Fig. 13 at (a) the step at $f_y^d/f_x^d = 2.412$ and (b) the step at $f_y^d/f_x^d = 2.51$.

jectories on the small step centered at $f_y^d/f_x^d = 2.412$ from Fig. 13. Here the particle moves at 60° for a distance of about $17a$, then jumps over to the next row, moves at 60° again, and then repeats the cycle of alternately jumping and moving. In Fig. 14(b), on the step just after $f_y^d/f_x^d = 2.51$ a similar motion is seen as in Fig. 14(a); however, the particle moves a distance of about $9a$ before jumping to the adjacent row. This staircase-type motion is similar to the dynamics just above the transverse depinning transition as shown in Fig. 6. In both these cases the particle moves predominantly along the symmetry angle which is 0° for the transverse depinning and 60° here, with periodic jumps into the next row. For the higher-order steps, the particle moves a shorter distance in the 60° direction before jumping to the next row.

V. STRONGLY INTERACTING PARTICLES

We next consider the case of driven particles with $q_d/q > 2.5$. In this regime we find that a significant number of dislocations are introduced into the system. In Fig. 15 we show V_y and V_x for $q_d/q = 5.0$. Here the curves are noisy with several sharp steps. No clearly defined locking regime is present; however, there are remnants of the $(1, 0)$ locking regime.

The smaller phase locking regions for drive angles less than 60° that were present at smaller q_d are completely washed out in Fig. 15. On these smallest steps, as illustrated in Fig. 8, the driven particle created the largest distortions in the surrounding lattice. As q_d is increased, dislocations appear first for the steps which produce the largest lattice distortions, and hence the smallest phase locking regions are smeared out first. This explains the disappearance of these phases at large q_d . Figure 15 shows that there is still an appreciable locking effect for the $m = 1, n = 0$ phase. The intermittent jumps in the velocities are due to the formation of dislocations, a process which abruptly changes the velocity of the driven particle. Additionally, a small number of dislocations remain in the colloid lattice for f_y^d/f_x^d below the $m = 1, n = 0$ phase. In Fig. 16 we show the trajectories for the system in Fig. 15 for $f_y^d/f_x^d = 1.0$. Here the trajectories are strongly disordered and in general do not overlap. For this value of drive a number of dislocations are created in the lattice. Some of the dislocations disappear when the lattice reorders once the driven particle moves past; however, some persist for long times. Since we are using periodic boundary

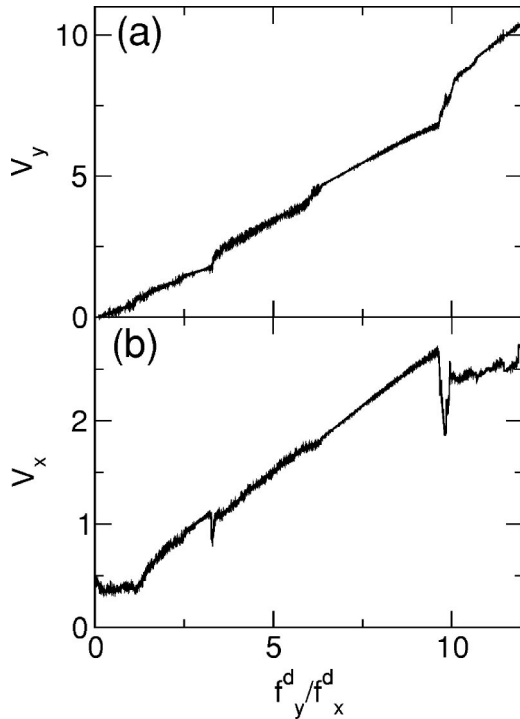


FIG. 15. (a) V_y vs f_y^d/f_x^d for $q_d/q=5$. (b) Corresponding V_x vs f_y^d/f_x^d .

conditions, the particle passes through the same region repeatedly and interacts with the persistent dislocations, which could make the flow more disordered. To address this we have performed the same simulations for larger systems and examined the trajectories before the particle comes back on its previous path. We find the same disordered flow, indicating that it is the process of dislocation creation which causes the particle trajectories to become disordered and not the existence of dislocations from a previous passage. We have also measured the power spectra in this case and find white noise rather than a narrow band signal.

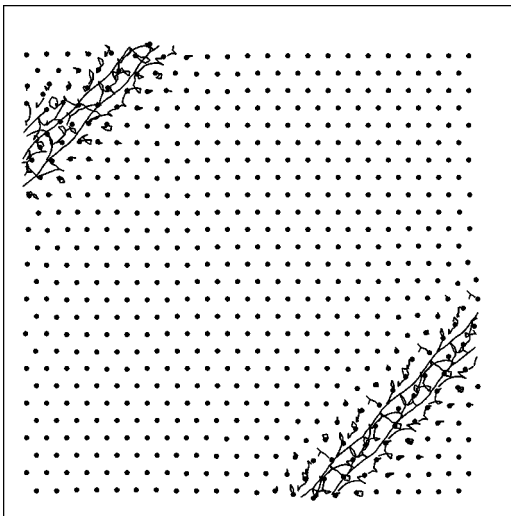


FIG. 16. Particles (black dots) and trajectories (black lines) for the system in Fig. 15 at $f_y^d/f_x^d=1.0$.

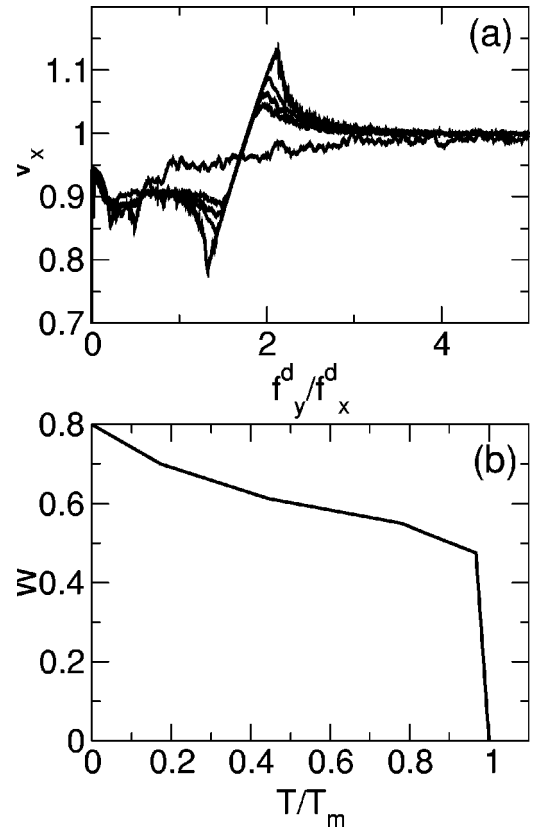


FIG. 17. (a) V_x vs f_y^d/f_x^d for varied $T/T_m=0.0, 0.44, 0.7, 0.9,$ and 1.01 . T_m is the temperature at which the nondriven lattice melts. The curve with the largest $(1,0)$ locking phase (centered at $f_y^d/f_x^d=1.7$) is $T=0.0$. The width of the $(1,0)$ locking phase decreases for increasing T . (b) Width W of the $(1,0)$ locking vs T/T_m for the system in Fig. 17(a).

VI. TEMPERATURE EFFECTS

In a real colloidal system, temperature effects will be relevant. For a triangular colloidal system at a finite density, there is a well-defined melting temperature T_m above which dislocations proliferate. We investigate the effects of the temperature on the locking up to T_m . We concentrate on the system with $q_d/q=0.5$ where locking is still clearly visible but the driven particle does not generate dislocations in the surrounding media at $T=0$. In Fig. 17(a) we show V_x for $T/T_m=0.0, 0.44, 0.7, 0.9,$ and 1.01 . For the lowest temperature, the width of the $(1,0)$ step is the largest. It decreases for higher T and disappears above T_m . Additionally, the initial dip in V_x for the transversely pinned phases is also reduced as the temperature increases. The higher-order locked regions for $f_y^d/f_x^d < 1.4$ become washed out for $T/T_m \geq 0.7$.

In Fig. 17(b) we plot the width W of the $(1,0)$ locking step from Fig. 17(a). Here the width decreases with increasing T and drops suddenly at T_m . This indicates that, even for relatively small particles, the locking effects should be observable in an experimental system all the way up to the melting transition of the colloidal lattice itself.

VII. SUMMARY

In summary, we have investigated the dynamics of driven particles moving through a triangular colloidal lattice for var-

ied orientations of the drive with respect to the symmetry of the colloidal lattice. This system, where the driven particle causes distortions in the surrounding colloidal lattice, differs from previously studied systems in which particles are driven through a lattice of *fixed* obstacles or traps. We find a series of locked phases as a function of drive angle where the particles prefer to move along certain symmetry directions. For driven particles that interact only weakly with the surrounding lattice, we find a devil's staircase structure. For larger driven particles, the locking effects become much more pronounced and the transitions into and out of the locked states become much sharper. These transitions can be accompanied by the creation of short-lived dislocations in the surrounding lattice. We also find some important features such as negative differential resistance in both the transverse and longitudinal velocities in the intermediate particle regime. As the charge of the driven particles increases, the

smallest locking regimes are lost when the main locking regimes grow and significant distortion of the surrounding lattice occurs. For larger particles, the locking effects are washed out when significant numbers of dislocations are created. Since the width of the locking steps depends strongly on the charge of the driven particle, our results may be useful as a method for particle separation techniques or electrophoresis. We have also studied the dynamics at the transitions into and out of the main locking states and find a staircaselike motion of the driven particle.

ACKNOWLEDGMENTS

We thank C. Bechinger, D. G. Grier, M. B. Hastings, P. Korda, X. S. Ling, A. Pertsinidis, and G. Spalding for useful discussions. This work was supported by the US DOE under Contract No. W-7405-ENG-36.

-
- [1] C. A. Murray and D. H. Van Winkle, *Phys. Rev. Lett.* **58**, 1200 (1987); A. E. Larsen and D. G. Grier, *ibid.* **76**, 3862 (1996); A. H. Marcus and S. A. Rice, *ibid.* **77**, 2577 (1996).
- [2] For reviews of colloidal matter, see C. A. Murray and D. G. Grier, *Am. Sci.* **83**, 238 (1995); H. Lowen, *J. Phys.: Condens. Matter* **13**, R415 (2001).
- [3] P. T. Korda, M. B. Taylor, and D. G. Grier, *Phys. Rev. Lett.* **89**, 128301 (2002).
- [4] E. R. Dufresne and D. G. Grier, *Rev. Sci. Instrum.* **69**, 1974 (1998); E. R. Dufresne, G. C. Spalding, M. T. Dearing, S. A. Sheets, and D. G. Grier, *ibid.* **72**, 1810 (2001); C. Bechinger, M. Brunner, and P. Leiderer, *Phys. Rev. Lett.* **86**, 930 (2001); J. E. Curtis, B. A. Koss, and D. G. Grier, *Opt. Commun.* **207**, 169 (2002).
- [5] M. P. MacDonald, G. C. Spalding, and K. Dholakia, *Nature (London)* **426**, 421 (2003); K. Ladavac, K. Kasza, and D. G. Grier, e-print cond-mat/0310396.
- [6] A. Gopinathan and D. G. Grier, e-print cond-mat/0311117.
- [7] For reviews of colloidal manipulation with optics, see K. Dholakia, G. Spalding, and M. MacDonald, *Phys. World* **15**, 31 (2002); D. G. Grier, *Nature (London)* **424**, 810 (2003).
- [8] T. A. J. Duke and R. H. Austin, *Phys. Rev. Lett.* **80**, 1552 (1998); D. Ertas, *ibid.* **80**, 1548 (1998); C.-F. Chou, R. H. Austin, O. Bakajin, J. O. Tegenfeldt, J. A. Castellino, S. S. Chan, E. C. Cox, H. Craighead, N. Darnton, T. Duke, J. Han, and S. Turner, *Electrophoresis* **21**, 81 (2000); R. H. Austin, N. Darnton, R. Huang, J. Sturm, O. Bakajin, and T. Duke, *Appl. Phys. A: Mater. Sci. Process.* **A75**, 279 (2002); L. R. Huang, P. Silberzan, J. O. Tegenfeldt, E. C. Cox, J. C. Sturm, R. H. Austin, and H. Craighead, *Phys. Rev. Lett.* **89**, 178301 (2002).
- [9] For a review of some related separation techniques, see J.-L. Viovy, *Rev. Mod. Phys.* **72**, 813 (2000).
- [10] C. Reichhardt and F. Nori, *Phys. Rev. Lett.* **82**, 414 (1999).
- [11] K. D. Fisher, D. Stroud, and L. Janin, *Phys. Rev. B* **60**, 15371 (1999).
- [12] V. I. Marconi, S. Candia, P. Balenzuela, H. Pastoriza, D. Domínguez, and P. Martinoli, *Phys. Rev. B* **62**, 4096 (2000); D. E. Shalom and H. Pastoriza, *Solid State Commun.* **126**, 379 (2003).
- [13] V. I. Marconi and D. Domínguez, *Phys. Rev. B* **63**, 174509 (2001).
- [14] A. V. Silhanek, L. Van Look, S. Raedts, R. Jonckheere, and V. V. Moshchalkov, *Phys. Rev. B* **68**, 214504 (2003); J. E. Villegas, E. M. Gonzalez, M. I. Montero, I. K. Schuller, and J. L. Vicent, *Phys. Rev. B* **68**, 224504 (2003).
- [15] G. Carneiro, *Phys. Rev. B* **62**, R14661 (2000); C. C. de Souza Silva and G. Carneiro, *ibid.* **66**, 054514 (2002).
- [16] J. Wiersig and K.-H. Ahn, *Phys. Rev. Lett.* **87**, 026803 (2001); J. Wiersig and K.-H. Ahn, *Physica E (Amsterdam)* **12**, 256 (2002).
- [17] E. Granato and S. C. Ying, *Phys. Rev. Lett.* **85**, 5368 (2000).
- [18] P. Haldas, D. Schaar, A. C. Levitt, and E. R. Weeks, e-print cond-mat/0308622.
- [19] J. A. Weiss, D. W. Oxtoby, D. G. Grier, and C. A. Murray, *J. Chem. Phys.* **103**, 1180 (1995).
- [20] T. Matsuda, K. Harada, H. Kasai, O. Kamimura, and A. Tonomura, *Science* **271**, 1393 (1996).
- [21] R. A. Quinn and J. Goree, *Phys. Rev. E* **64**, 051404 (2001).
- [22] C. Reichhardt and C. J. Olson, *Phys. Rev. Lett.* **89**, 078301 (2002); **88**, 248301 (2002); C. J. Olson Reichhardt and C. Reichhardt, *J. Phys. A* **36**, 5841 (2003).
- [23] M. B. Hastings, C. J. Olson Reichhardt, and C. Reichhardt, *Phys. Rev. Lett.* **90**, 098302 (2003).
- [24] C. Reichhardt and C. J. Olson Reichhardt, *Phys. Rev. Lett.* **90**, 095504 (2003).
- [25] D. S. Fisher, *Phys. Rev. B* **31**, 1396 (1985).
- [26] D. Domínguez, *Phys. Rev. Lett.* **72**, 3096 (1994); C. Reichhardt and C. J. Olson, *ibid.* **89**, 078301 (2002).